

XMM-Newton observation of the cooling-flow cluster Abell 478

Jelle de Plaa,¹ Jelle S. Kaastra,¹ Takayuki Tamura,^{1,2} Mariano Mendez,¹ John R. Peterson,³ Etienne Pointecouteau,⁴ and Monique Arnaud⁴

¹ *SRON National Institute for Space Research, Utrecht, The Netherlands*

² *ISAS Institute of Space and Astronautical Science, Kanagawa, Japan*

³ *Astrophysics Laboratory, Columbia University, New York, USA*

⁴ *CEA/DSM/DAPNIA Saclay, Service d'Astrophysique, Gif-sur-Yvette, France*

We present the results of an *XMM-Newton* observation of the hot cooling-flow cluster Abell 478 performed in Guaranteed Time. Using the large effective area and high spectral resolution of *XMM-Newton* in the soft X-ray band, we derive the temperature profile and abundances in the cluster. We conclude that we need a multi-temperature model to fit the spectrum in the core of the cluster.

1. Introduction

The cluster of galaxies Abell 478 (Fig. 1) is a good example of a highly relaxed cluster. Earlier X-ray observations by *Ginga* and *Einstein* (Johnstone et al. 1992), *ROSAT* (Allen et al. 1993; White et al. 1994), *ASCA* (Markevitch et al. 1998; White 2000) and *Chandra* (Sun et al. 2003) show a significant excess of X-ray emission in the core, suggesting the presence of a massive cooling-flow. The observations performed by missions with sufficient spatial resolution (e.g. *ROSAT*, *ASCA* and *Chandra*) are consistent with a radial temperature decrease toward the core. In a recent *Chandra* observation an X-ray cavity was discovered in the core which seems to be associated with a lobed radio source (Sun et al. 2003).

Because Abell 478 is one of the hottest clusters in the X-ray sky, its spectrum is dominated by thermal Bremsstrahlung. In order to be able to study the line

emission we used the large effective area and spectral resolution of *XMM-Newton* (Jansen et al. 2001). In this paper we present the results from the spatially resolved spectra obtained with the European Photon Imaging Camera (EPIC, Turner et al. 2001) and the high resolution spectra from the Reflection Grating Spectrometer (RGS, den Herder et al. 2001).

2. Observations

The observation of Abell 478 was performed as part of the Guaranteed Time program on February 15 2002 and had a total duration of 126 ks. Both EPIC MOS cameras were operated in Full Frame mode and the EPIC pn camera in Extended Full Frame mode. For all EPIC cameras the thin filter was used.

For the initial data processing we used the 5.4.1 version of the XMM Science Analysis System (SAS) software. To correct for enhanced and variable background due to soft proton flares the data were filtered using upper and lower count-rate thresholds. The thresholds were calculated analogous to the method used in Pratt & Arnaud (2002). This procedure resulted in useful exposure times of 81.3 ks (MOS), 53.8 ks (pn) and 123 ks (RGS).

3. EPIC Analysis & Results

3.1. Temperature and Absorption

The temperature and interstellar absorption profiles were obtained from spectra extracted from circular annuli. An offset pointing was used to obtain more accurate results for the edge of the cluster. Projection and PSF corrections were not applied to the spectra. We fitted the spectra using an absorbed, redshifted thermal emission spectrum (MEKAL) model in XSPEC with N_{H} , z and kT as free parameters as well as the normalization for each detector. This resulted in an acceptable χ^2 for each annulus. Fig. 3 shows the radial temperature profile for Abell 478 and in Fig. 4 the total radial absorption is shown. The column density gradually diminishes toward the edge due to a molecular cloud.

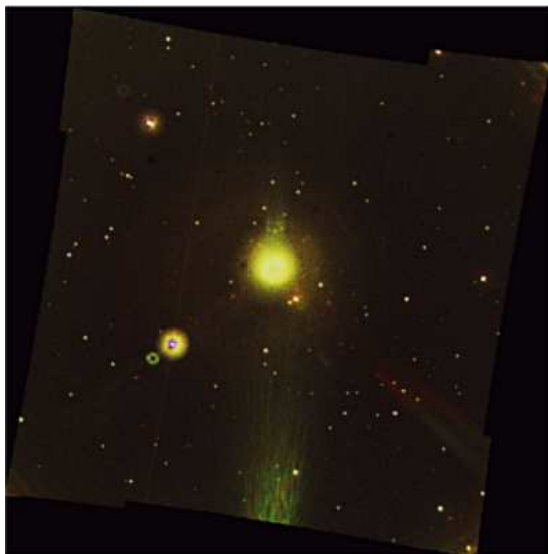


FIG. 1.— Optical/UV image of Abell 478 obtained with the Optical Monitor (OM) aboard *XMM-Newton*.

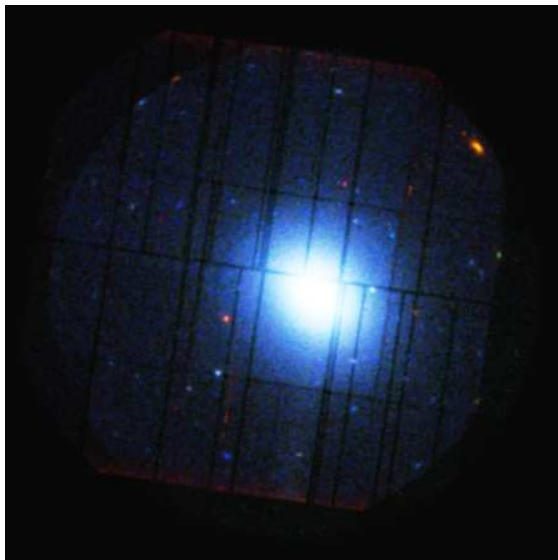


FIG. 2.— EPIC image of Abell 478. The field of view is approximately $30' \times 30'$. (Energy ranges: Red = 0.2–1.0 keV, Green = 1.0–2.5 keV, Blue = 2.5–10. keV)

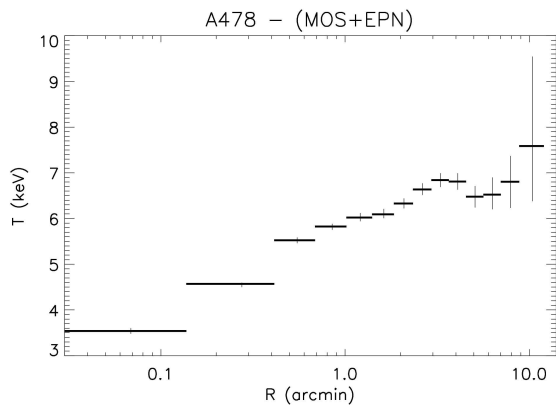


FIG. 3.— Temperature profile of Abell 478 derived from EPIC single-temperature fits.

3.2. Abundances

For the determination of the abundance profiles we used a different method. Because the cluster is slightly elongated (see Fig. 2), we extracted the source and background spectra from elliptical annuli. The EPIC background spectra were extracted from the background event files provided by Read & Ponman (2003). Furthermore, we corrected the effective area for the blurring effect of the PSF and removed bright point sources. The spectral analysis was performed with the SPEX package (Kaastra et al. 2003a).

Because the source is partly obscured by a molecular cloud (see Fig. 5), we used two absorption components. The N_{H} of the first component was fixed to the galactic 21 cm value of $1.51 \times 10^{21} \text{ cm}^{-2}$ provided by the HEASARC N_{H} web tool (Dickey & Lockman 1990). In the second component the N_{H} and the oxygen abundance were left free to account for the excess absorption caused by the molecular cloud and calibration uncertainties in the oxygen edge.

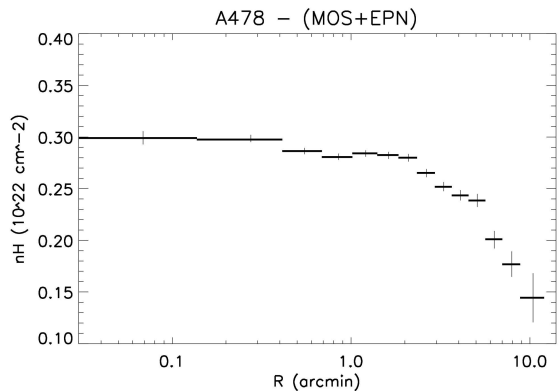


FIG. 4.— Total column density profile (EPIC single-temperature fit)

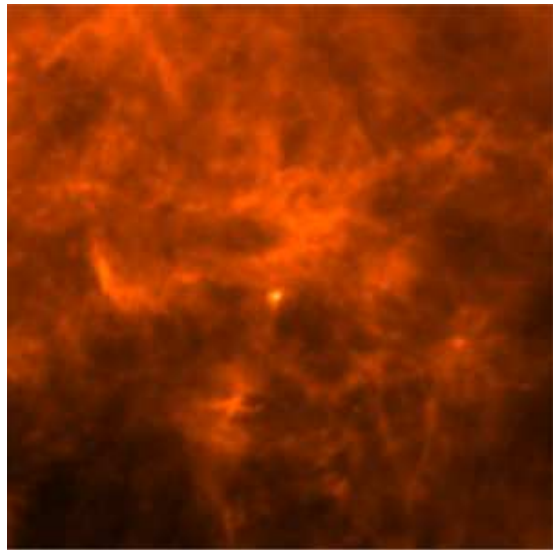


FIG. 5.— IRAS $100\mu\text{m}$ image of the Abell478 region from Skyview. The dimensions of the image are $7.5^\circ \times 7.5^\circ$ (Wheelock et al. 1991). Abell 478 is at the center of the image.

We fitted the spectra with a single-temperature model in all annuli. Abundance profiles measured by EPIC are shown in Fig. 6.

The χ^2 values for the single temperature fits were higher in the core, therefore the spectra were also fitted with a differential emission measure model (DEM). In this particular model the emission measure is distributed as a function of temperature as shown in Eq. (1):

$$\frac{dY}{dT} = \begin{cases} cT^\alpha & T < T_{\text{max}} \\ 0 & T > T_{\text{max}} \end{cases} \quad (1)$$

This model called *wdem* is an empirical parametrization of the DEM distribution found in the cores of many clusters (Kaastra et al. 2003b). In this form the limit $\alpha \rightarrow \infty$ yields the isothermal model. For convenience we will use $1/\alpha$ in this paper, because then the isothermal model is obtained when $1/\alpha = 0$.

For the determination of the radial abundances we concentrated on the core of the cluster and did not use the offset pointing. Beyond $4'$ the χ^2 value jumps to nearly two times the d.o.f. because the signal becomes similar in

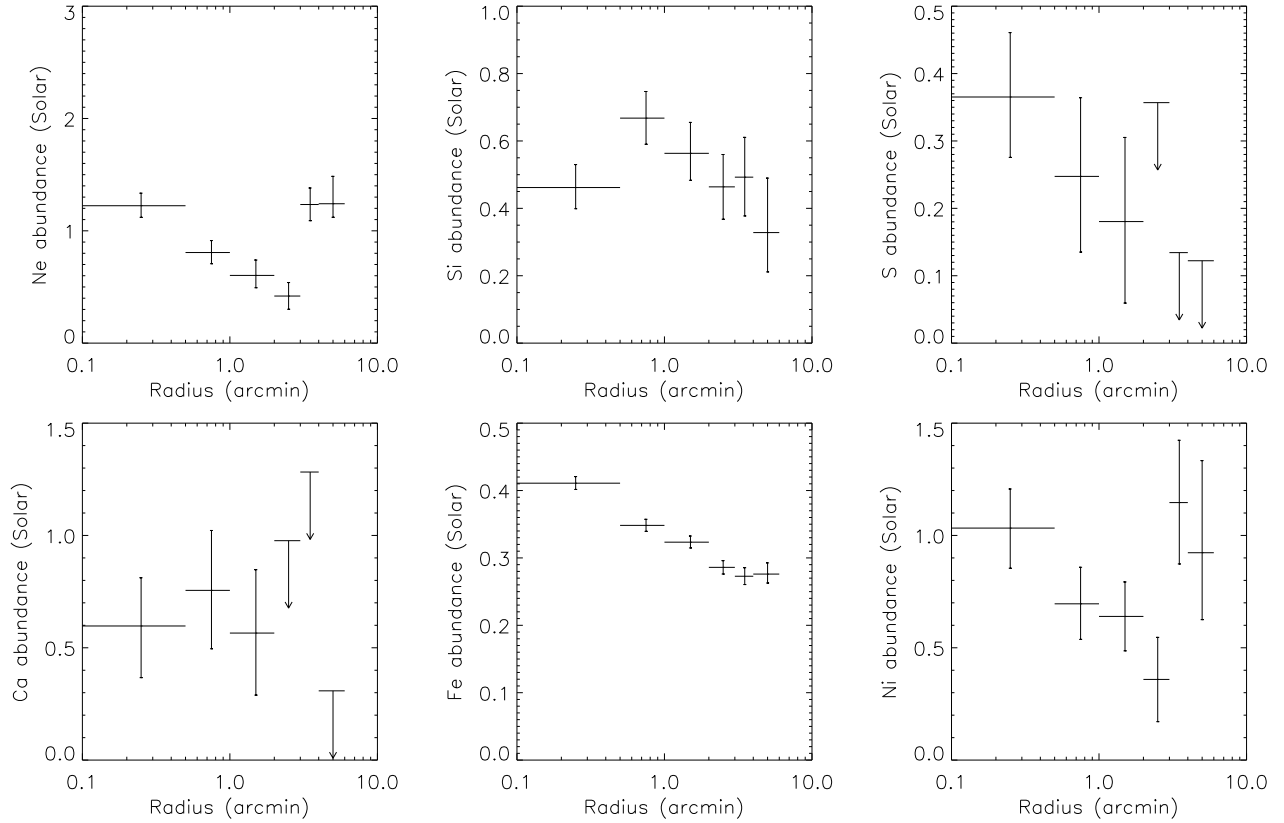


FIG. 6.— Radial abundance profiles from the single temperature fits.

TABLE 1. RGS AND EPIC SPECTRAL FITS (*wdem*; 0–0'5).

	RGS	EPIC	Unit
$\chi^2/\text{d.o.f}$	877/752	701/526	
$N_{\text{H,excess}}^a$	1.68 ± 0.07	$2.35^{+0.02}_{-0.06}$	10^{21} cm^{-2}
O_{edge}^b	0.44 ± 0.07	0.08 ± 0.02	Z_{solar}
T_{max}	$10.0^{+2.0}_{-1.5}$	$7.5^{+0.3}_{-0.10}$	keV
$1/\alpha$	1.1 ± 0.2	$1.3^{+0.19}_{-0.15}$	
O	0.13 ± 0.06	< 0.06	Z_{solar}
Ne	0.48 ± 0.12	0.32 ± 0.09	Z_{solar}
Mg	0.18 ± 0.12	< 0.12	Z_{solar}
Si		0.45 ± 0.05	Z_{solar}
S		0.45 ± 0.08	Z_{solar}
Ca		0.9 ± 0.2	Z_{solar}
Fe	$0.55^{+0.18}_{-0.12}$	0.42 ± 0.01	Z_{solar}
Ni		0.78 ± 0.17	Z_{solar}

NOTE. — Errors are given at the 1σ confidence level, and the $<$ -sign denotes a 2σ upper limit.

^athe excess absorption on top of the galactic absorption which was fixed at $1.51 \times 10^{21} \text{ cm}^{-2}$

^bThe abundance of oxygen in the absorption component was left free to fit the oxygen edge near 0.5 keV.

strength compared to the background. Therefore, the fit becomes very sensitive to systematic effects. Moreover,

the excess absorption from the molecular cloud influences the extragalactic soft X-ray background component and introduces an extra systematic effect in the background. Because of this effect and the high χ^2 outside the 4' radius we ignore these bins in our present discussion.

4. RGS Analysis & Results

We obtained a reasonable fit for the RGS instrument using the *wdem* component described in Eq. 1 (see Table 1 and Fig. 7). With a χ^2 of 877/752 the *wdem* fit is just marginally better than the single temperature fit with a χ^2 of 887/754. Unfortunately, the oxygen abundance is not well determined because the O VIII line complex is near a bad-column on the CCD of RGS1 and falls in the dead area of RGS2. The Fe-L complex near 12 Å was detected and resolved as well.

5. Conclusions

Because of the excellent sensitivity of *XMM-Newton* we can conclude that the core of this hot cluster is best fitted with a DEM model. The fact that the *wdem* fit to the RGS data is just marginally better than a fit using a single-temperature component might be due to the small number of emission lines detected. Because of the high Bremsstrahlung continuum the number of lines on which the DEM distribution can be constrained is of course very small. Therefore, the broader band of the EPIC is much better in this case for determining the temperature structure.

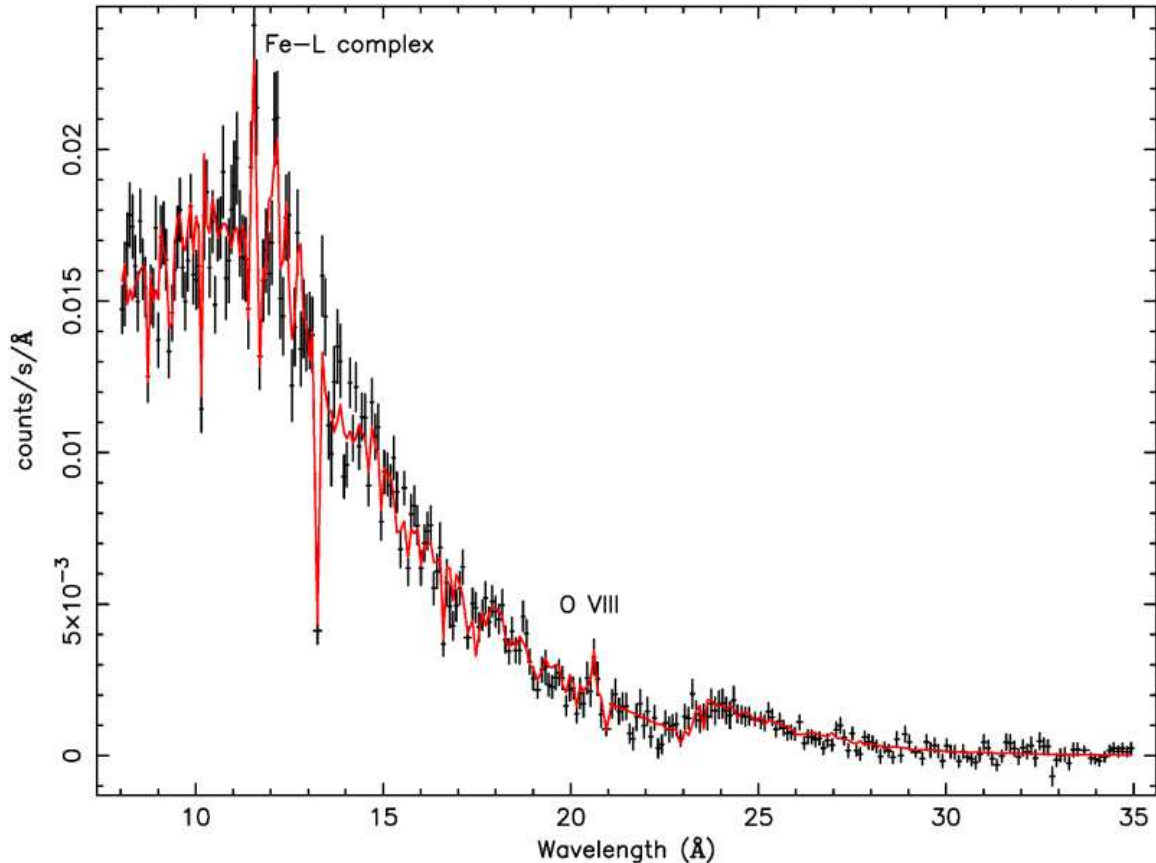


FIG. 7.— Averaged RGS spectrum of Abell 478 fitted with the DEM model component described in Eq. (1)

This work is based on observations obtained with *XMM-Newton*, an ESA science mission with instruments and contributions directly funded by ESA member states and the USA (NASA). The Space Research Organization

of the Netherlands (SRON) is supported financially by NWO, the Netherlands Organization for Scientific Research.

References

- Allen, S. W., Fabian, A. C., Johnstone, R. M., White, D. A., Daines, S. J., Edge, A. C., & Stewart, G. C. 1993, *MNRAS*, 262, 901
- den Herder, J. W., Brinkman, A. C., Kahn, S. M., Branduardi-Raymont, G., Thomsen, K., Aarts, H., Audard, M., Bixler, J. V., den Boggende, A. J., Cottam, J., Decker, T., Dubbeldam, L., Erd, C., Gouloze, H., Güdel, M., Guttridge, P., Hailey, C. J., Janabi, K. A., Kaastra, J. S., de Korte, P. A. J., van Leeuwen, B. J., Mauche, C., McCalden, A. J., Mewe, R., Naber, A., Paerels, F. B., Peterson, J. R., Rasmussen, A. P., Rees, K., Sakelliou, I., Sako, M., Spodek, J., Stern, M., Tamura, T., Tandy, J., de Vries, C. P., Welch, S., & Zehnder, A. 2001, *A&A*, 365, L7
- Dickey, J. M. & Lockman, F. J. 1990, *ARA&A*, 28, 215
- Jansen, F., Lumb, D., Altieri, B., Clavel, J., Ehle, M., Erd, C., Gabriel, C., Guainazzi, M., Gondoin, P., Much, R., Munoz, R., Santos, M., Schartel, N., Texier, D., & Vacanti, G. 2001, *A&A*, 365, L1
- Johnstone, R. M., Fabian, A. C., Edge, A. C., & Thomas, P. A. 1992, *MNRAS*, 255, 431
- Kaastra, J. S., Mewe, R., & Raassen, A. A. J. 2003a, in *New Visions of the X-ray Universe in the XMM-Newton and Chandra Era*, ed. F. A. Jansen, Vol. in press (ESA)
- Kaastra, J. S., Tamura, T., Peterson, J. R., Bleeker, J., Ferrigno, C., Kahn, S. M., Paerels, F. B. S., Piffaretti, R., Branduardi-Raymont, G., & Böhringer, H. 2003b, *A&A*, in press.
- Markevitch, M., Forman, W. R., Sarazin, C. L., & Vikhlinin, A. 1998, *ApJ*, 503, 77
- Pratt, G. W. & Arnaud, M. 2002, *A&A*, 394, 375
- Read, A. M. & Ponman, T. J. 2003, *A&A*, 409, 395
- Sun, M., Jones, C., Murray, S. S., Allen, S. W., Fabian, A. C., & Edge, A. C. 2003, *ApJ*, 587, 619
- Turner, M. J. L., Abbey, A., Arnaud, M., Balasini, M., Barbera, M., Belsole, E., Bennie, P. J., Bernard, J. P., Bignami, G. F., Boer, M., Briel, U., Butler, I., Cara, C., Chabaud, C., Cole, R., Collura, A., Conte, M., Cros, A., Denby, M., Dhez, P., Di Coco, G., Dowson, J., Ferrando, P., Ghizzardi, S., Gianotti, F., Goodall, C. V., Gretton, L., Griffiths, R. G., Hainaut, O., Hochedez, J. F., Holland, A. D., Jourdain, E., Kendziorra, E., Lagostina, A., Laine, R., La Palombara, N., Lortholary, M., Lumb, D., Marty, P., Molendi, S., Pigot, C., Poindron, E., Pounds, K. A., Reeves, J. N., Reppin, C., Rothenflug, R., Salvatat, P., Sauvageot, J. L., Schmitt, D., Sembay, S., Short, A. D. T., Spragg, J., Stephen, J., Strüder, L., Tiengo, A., Trifoglio, M., Trümper, J., Vercellone, S., Vigroux, L., Villa, G., Ward, M. J., Whitehead, S., & Zonca, E. 2001, *A&A*, 365, L27
- Wheelock, S., Chillemi, J., Gautier, N., Gregorich, D., Kester, D., McCallon, H., Oken, C., White, J., & Chester, T. 1991, *BAAS*, 23, 908
- White, D. A. 2000, *MNRAS*, 312, 663
- White, D. A., Fabian, A. C., Allen, S. W., Edge, A. C., Crawford, C. S., Johnstone, R. M., Stewart, G. C., & Voges, W. 1994, *MNRAS*, 269, 589